

# A Color LED Driver Implemented by the Active Clamp Forward Converter

C. H. Chang, H. L. Cheng, C. A. Cheng, E. C. Chang\*

Power Electronics Laboratory, Department of Electrical Engineering  
I-Shou University, Kaohsiung City 84001, Taiwan  
\*enchihchang@isu.edu.tw

## ABSTRACT

Because light emitting diodes (LEDs) have the advantages of dc working voltage, high luminescent efficiency, short ignition time, high reliability and pollution free, they have substituted for incandescent bulbs and fluorescent lamps gradually. In order to simplify circuit complexity, an active clamp forward converter with the sequential color display (SCD) control is proposed to drive red, green and blue (RGB) LED arrays. The proposed converter has zero-voltage switching (ZVS) operations of both the main switch and the auxiliary switch, resulting in high system efficiency. Driving RGB LED arrays sequentially by one converter can save components and reduce cost significantly. Additionally, the pulse-width modulation (PWM) control is applied to achieve a large chromaticity variation. The circuit operations are analyzed in detail and the circuit parameters are designed based on the practical considerations. Finally, an illustrative example is implemented to demonstrate the feasibility and validity of the proposed LED driver.

Keywords: Light emitting diode (LED), active clamp forward converter, sequential color display (SCD).

## 1. Introduction

Recently, light emitting diodes (LEDs) have substituted for incandescent bulbs and fluorescent lamps gradually in the residential, industrial and commercial lighting applications [1], because they have the advantages of dc working voltage, high luminescent efficiency, short ignition time, high reliability and pollution free, etc. Moreover, since mixing multi-coloured LEDs can provide a large chromaticity variation, LEDs are progressively used in outdoor landscape lighting systems as well.

Figure 1 shows the block diagram of a photovoltaic powered landscape lighting system, in which an isolated DC/DC converter is used to fulfill a step-down conversion, govern the current through LED arrays and provide the electrical isolation of safety requirements. Generally, a colored LED module is composed of red, green and blue (RGB) LED arrays. Since RGB LEDs have different electrical characteristics, three isolated DC/DC converters are required to regulate the current through each LED arrays [2]. Therefore, the number of power components will become triple, resulting in large volume, high cost and low reliability.

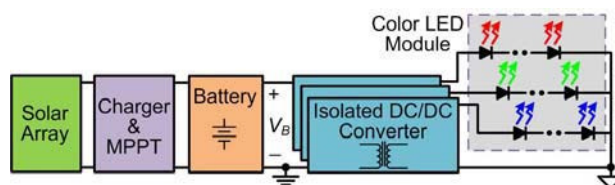


Figure 1. The block diagram of a photovoltaic powered landscape lighting system.

In the literature [3, 4], a sequential color scanning scheme was proposed to reduce power consumption. LEDs are very suitable for a sequential color display (SCD) due to their fast response. When LEDs are displayed intermittently with high frequency, human cannot observe the darkness of short time intervals. The SCD control has been applied in a color LED backlight driving system for liquid crystal display (LCD) panels [5], [6], in which RGB LED arrays are sequentially driven by the same DC/DC converter.

Many isolated DC/DC converters for RGB LED driving, such as flyback and forward converters, have been presented in the literature [3, 5].

However, their hard-switching operations reduce conversion efficiency and induce electromagnetic interference (EMI) noise. This paper proposes an active clamp forward converter [7 – 9] with SCD control as the color LED driver for a photovoltaic powered landscape lighting system. For this driver, due to saving transformers, power switches, control ICs and energy storage components, the circuit complexity can be simplified, and the system volume and cost can be significantly reduced. With accurate analysis and design, both of the main switch and the auxiliary switch can turn on under zero-voltage switching (ZVS), leading to higher system efficiency and lower EMI noise. Besides, the pulse-width modulation (PWM) control is applied to change the luminance of RGB LEDs so that a large chromaticity variation can be achieved. The operation principles are addressed. Experimental results of a 100 W laboratory prototype are used to verify the feasibility and validity of the theoretical predictions.

## 2. Operation principles

The proposed color LED driver, as shown in figure 2, consists of an active clamp forward converter and RGB LED arrays with SCD control. In this section, the operation principles of the SCD control and the proposed converter are introduced briefly in the following.

### 2.1 Sequential color display control

To achieve SCD control, RGB LED arrays are connected in series with the switches  $S_R$ ,  $S_G$  and  $S_B$ , respectively. The switches are driven with phase-shift manner, as illustrated in figure 3, in which  $V_{GS\_R}$ ,  $V_{GS\_G}$  and  $V_{GS\_B}$  are their gate signals with the switching frequency  $f_m$ . The frequency of the driving signals  $V_{GS1}$  and  $V_{GS2}$  in the active clamp forward converter is  $f_s$  which should be much higher than  $f_m$ . The voltages  $V_{o\_R}$ ,  $V_{o\_G}$  and  $V_{o\_B}$  are the forward voltage of RGB LED arrays, respectively. The currents  $i_R$ ,  $i_G$  and  $i_B$  are their corresponding driving currents.

Assuming that the currents  $i_R$ ,  $i_G$  and  $i_B$  have the same amplitude  $I_P$  at full-load condition, the maximum average output-current  $I_{o,avg}$  of a conventional RGB LED driver is  $3I_P$ . For the proposed driver, if the maximum duty cycle of the driving signals  $V_{GS\_R}$ ,  $V_{GS\_G}$  and  $V_{GS\_B}$  are  $D_{max}$ , then the maximum average output-current  $I_{o,avg}$  is

$$I_{o,avg} = I_P \times D_{max} \times 3 \tag{1}$$

Because  $D_{max}$  is 33.33% in the proposed driver,  $I_{o,avg}$  is only equal to  $I_P$ . Therefore, the required output-power of the proposed driver is only one-third of that of a conventional driver, which results in energy saving significantly.

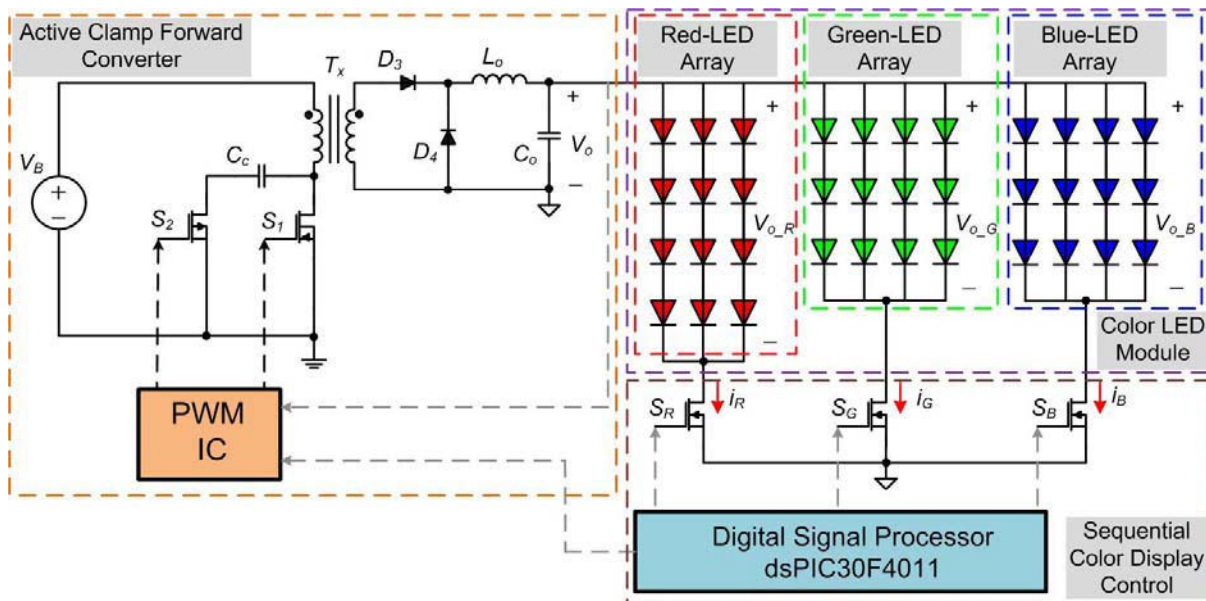


Figure 2. The conceptual circuit of the proposed color LED driver with SCD control.

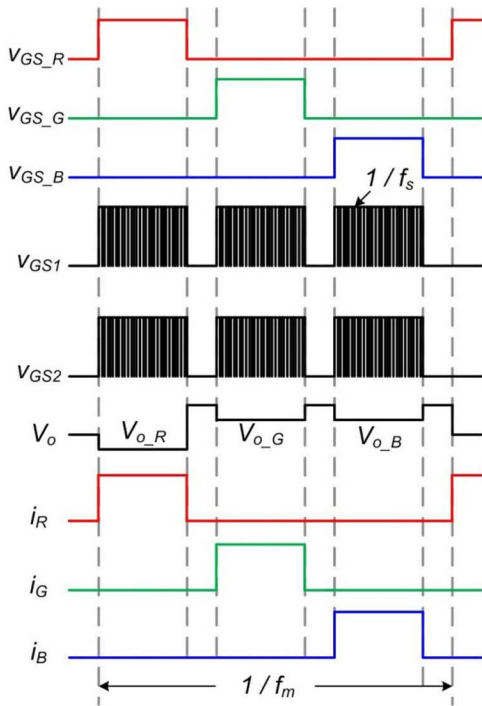


Figure 3. Driving signals and conceptual key waveforms of the SCD control.

In the proposed system, the red, green and blue LED arrays are driven by the same converter sequentially, leading to small volume, low cost and high reliability. All of the driving signals  $V_{GS\_R}$ ,  $V_{GS\_G}$  and  $V_{GS\_B}$  are produced by the digital signal processor (dsPIC30F4011). The luminance of each LED array is dimmable by modulating the duty of its driving signal, so as the color of the RGB-LED module is variable. The output capacitor  $C_o$  with low capacitance is used in the converter so that the output voltage can vary promptly according to the forward voltage of each LED array.

### 2.2 Active clamp forward converter

Figure 4 shows the circuit diagram of the active clamp forward converter. Each active switch  $S_1$  ( $S_2$ ) is composed of an MOSFET  $Q_1$  ( $Q_2$ ) and its intrinsic anti-parallel diode  $D_1$  ( $D_2$ ). The forward converter is formed by the main switch  $S_1$ , transformer  $T_x$ , forward diode  $D_3$ , freewheel diode  $D_4$ , output inductor  $L_o$ , and output capacitor  $C_o$ . Instead of the reset winding in traditional forward converter, the auxiliary switch  $S_2$  and the clamping

capacitor  $C_c$  are used to reset the residual flux of transformer. The residual energy of magnetizing inductor  $L_m$  can be restored to the input voltage source. Both of the main switch  $S_1$  and the auxiliary switch  $S_2$  can turn on under ZVS, resulting in low switching losses and high system efficiency.

For simplifying the analysis of operation principles, following conditions are made:

- 1) All components are ideal.
- 2) The capacitance of  $C_c$  is much higher than that of the intrinsic capacitor  $C_{ds}$ , and the inductance of  $L_m$  is much higher than that of the leakage inductor  $L_r$ .
- 3)  $L_o$  and  $C_o$  are large enough so that the output voltage  $V_o$  and output current  $I_o$  can be regarded as constant.
- 4) The dead time between the driving signals of  $S_1$  and  $S_2$  is very short and negligible. The turn-on intervals of  $S_1$  and  $S_2$  are considering as  $DT_s$  and  $(1-D)T_s$ , in which  $T_s$  is the switching period in steady-state operation.

According to the volt-second balance concept, the relation of input voltage  $V_B$  and the voltage across clamping capacitor  $v_c$  can be expressed as

$$V_B DT_s = (v_c - V_B)(1-D)T_s \tag{2}$$

Arranging Eq. 2 yields

$$v_c = \frac{1}{(1-D)} V_B \tag{3}$$

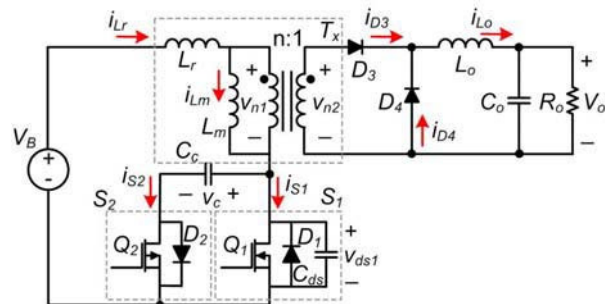


Figure 4. Circuit diagram of the active clamp forward converter.

Eq. 3 indicates that  $v_c$  is the output of boost-type operation with input voltage  $V_B$ . When  $S_1$  turns off and  $S_2$  turns on, the voltage across main switch  $v_{ds1}$  will be equal to  $v_c$  and determined as

$$v_{ds1} = v_c = \frac{1}{(1-D)} V_B \quad (4)$$

Figure 5 shows the theoretical waveforms of the active clamp forward converter, which is divided into nine operation modes within one switching period. The operation principle of each mode will be introduced referring to the equivalent circuits shown in figure 6.

**Mode 1 ( $t_0 \sim t_1$ ):** At the moment  $t = t_0$ , the switch  $S_1$  is turning on, and the switch  $S_2$  is turning off. Since the voltage across magnetizing inductor  $v_{n1}$  is equal to  $V_B$ , its current  $i_{Lm}$  increases linearly. The voltage across secondary winding  $v_{n2}$  is  $V_B / n$  so that the forward diode  $D_3$  turns on and the freewheel diode  $D_4$  turns off. The input voltage source charges output inductor  $L_o$  through the transformer  $T_x$  and  $D_3$ . This mode ends while the gate signal of  $S_1$  disappears.

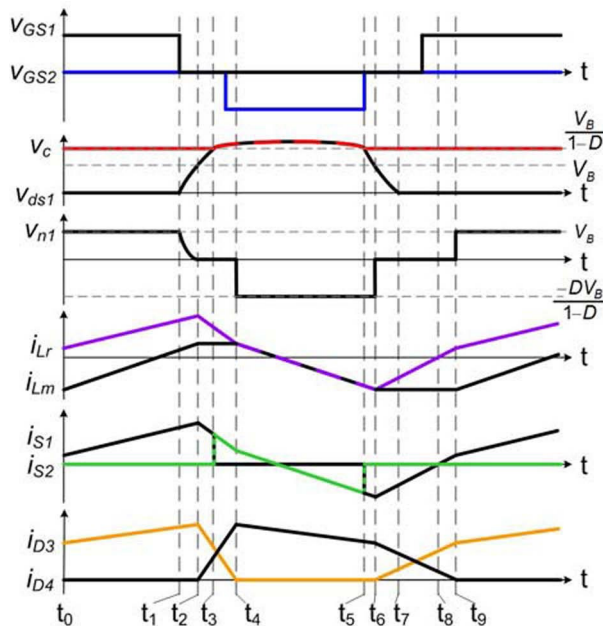


Figure 5. Theoretical waveforms of the active clamp forward converter.

**Mode 2 ( $t_1 \sim t_2$ ):** At the moment  $t = t_1$ , the main switch  $S_1$  turns off, and the current  $i_{Lr}$  charges the intrinsic capacitor  $C_{ds}$  of main switch. The voltage  $v_{ds1}$  increases, and the voltage  $v_{n1}$  decreases. This mode ends while  $v_{ds1}$  reaches  $V_B$ .

**Mode 3 ( $t_2 \sim t_3$ ):** At the moment  $t = t_2$ , the voltage  $v_{n1}$  reaches zero so that  $D_3$  and  $D_4$  are both turn-on. Since the diode current  $i_{D3}$  decreases, the leakage inductor current  $i_{Lr}$  decreases as well. The magnetizing inductor current  $i_{Lm}$  remains the same. This mode ends while  $v_{ds1}$  reaches  $V_B / (1-D)$ .

**Mode 4 ( $t_3 \sim t_4$ ):** At the moment  $t = t_3$ , the main switch  $S_1$  turns off. The current  $i_{Lr}$  flows through anti-parallel diode  $D_2$  to transfer energy to the clamping capacitor  $C_c$ , which provides ZVS operation for the auxiliary switch  $S_2$  turn-on. Gate signal of  $S_2$  should be applied during this mode. This mode ends while  $i_{D3}$  reaches zero.

**Mode 5 ( $t_4 \sim t_5$ ):** At the moment  $t = t_4$ , because the current  $i_{D3}$  is zero, the inductor  $L_m$  is in series with  $L_r$  and participates in the resonance with  $C_c$ . The voltage  $v_{n1}$  is  $DV_B / (1-D)$  with reverse polarity. The resonant current  $i_{Lr}$  is equal to the current  $i_{Lm}$  and remains decreasing. While  $i_{Lr}$  becomes negative during this mode, the energy of  $L_m$  will be restored to the input voltage source. This mode ends while the gate signal of  $S_2$  disappears.

**Mode 6 ( $t_5 \sim t_6$ ):** At the moment  $t = t_5$ , the auxiliary switch  $S_2$  turns off, and the resonant current  $i_{Lr}$  follows through the intrinsic capacitor  $C_{ds}$  to discharge it. This mode ends while the voltage  $v_{ds1}$  decreases to  $V_B$ .

**Mode 7 ( $t_6 \sim t_7$ ):** At the moment  $t = t_6$ , the voltage  $v_{ds1}$  is equal to  $V_B$  so that the voltage  $v_{n1}$  becomes zero again. Since  $D_3$  are turning on now, its current  $i_{D3}$  increases and the current  $i_{Lr}$  increases as well. The magnetizing inductor current  $i_{Lm}$  remains the same. This mode ends while  $v_{ds1}$  reaches zero.

**Mode 8 ( $t_7 \sim t_8$ ):** At the moment  $t = t_7$ , the current  $i_{Lr}$  flows through anti-parallel diode  $D_1$  to transfer energy back to the input voltage source, which provides ZVS operation for the main switch  $S_1$  turn-on. Gate signal of  $S_1$  should be applied during this mode. The current  $i_{Lr}$  increases from negative with the slope of  $V_B / L_r$ . This mode ends while  $i_{Lr}$  reaches zero.



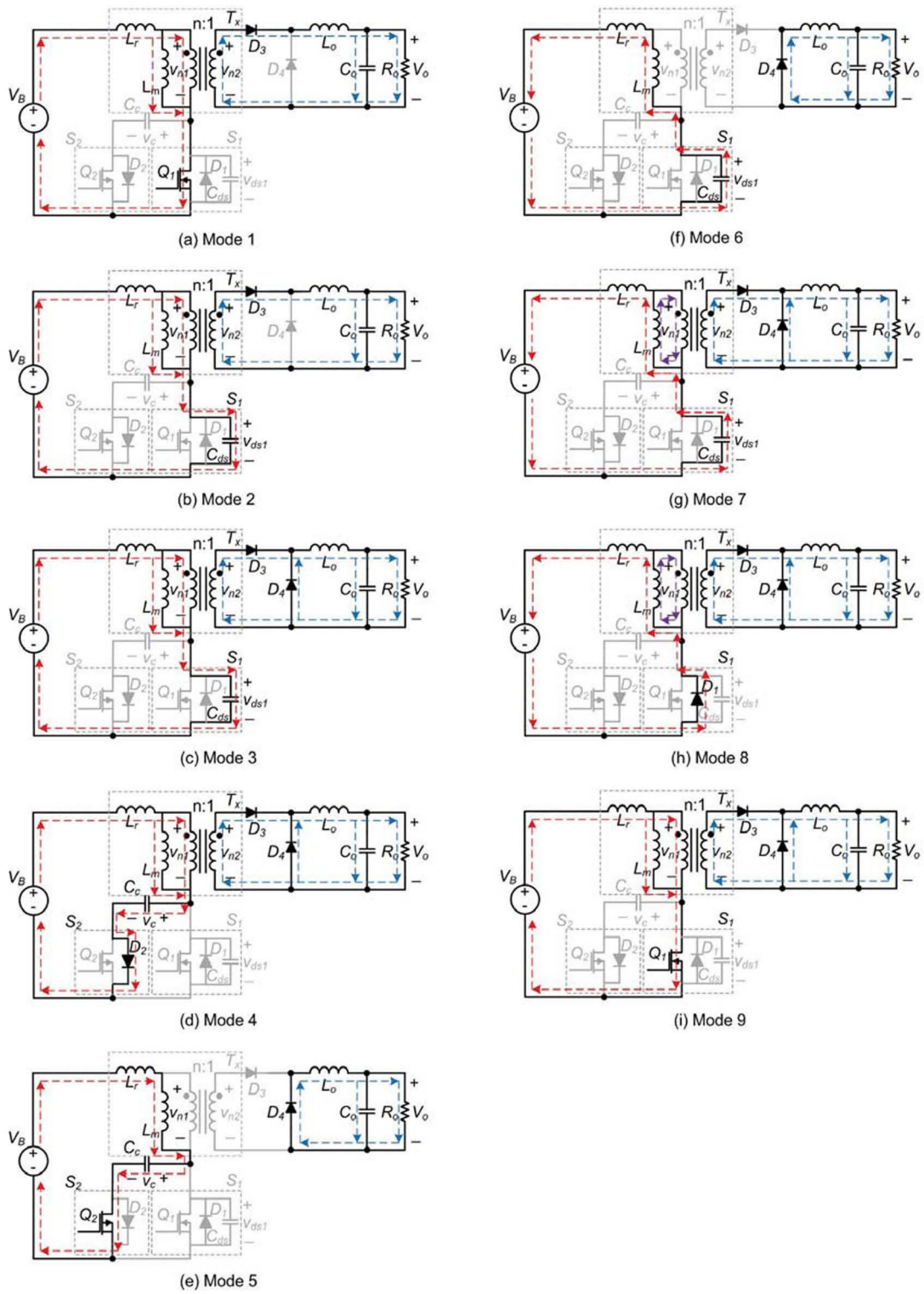


Figure 6. Equivalent circuits of operation modes.

Mode 9 ( $t_8 \sim t_9$ ): At the moment  $t = t_8$ , the current  $i_{Lr}$  becomes positive. The current  $i_{D4}$  is decreasing continuously, and this mode ends when  $i_{D4}$  reaches zero. When the diode  $D_4$  is turned off at  $t = t_9$ , the operation goes to Mode 1 of the next high-frequency switching cycle.

### 3. Design procedures

Based on the operation principles presented previously, the proposed color LED driver with the specifications listed in table 1 is taken as an illustrative example. The designed procedures of the active clamp forward converter are described as follows.

Step 1-Select  $f_s$  and  $D$ : Select the switching frequency  $f_s$  as 150 kHz. For the normal operation condition with 24 V battery voltage and full load output, the duty ratio  $D$  of the main switch  $S_1$  is determined as 0.5.

Step 2-Determine  $n$ : Considering that the forward voltage  $V_f$  of the diode  $D_3$  is around 0.7 V, the minimum turn ratio ( $n$ ) of the transformer  $T_x$  can be determined as

$$n \geq \frac{V_B \cdot D}{(V_o + V_f)} \cong 0.99 \quad (5)$$

In the illustrative case, ( $n$ ) is set as 1.

Step 3-Determine  $L_o$ : In order to minimize the output ripple current and reduce the current stress of power components, we select 10% of maximum output current as the boundary condition. The boundary inductance of  $L_o$  can be obtained as

$$L_{oB} = \frac{V_o \cdot (1-D)}{2 \cdot I_{oB} \cdot f_s} \cong 95 \mu\text{H} \quad (6)$$

In the illustrative case,  $L_o$  is set at 100  $\mu\text{H}$ .

Step 4-Determine  $C_o$ : While output inductance  $L_o$  is determined, considering that the specification of  $\Delta V_o$  is 10 mV, the capacitance of  $C_o$  can be obtained

$$C_o = \frac{(1-D)}{8L_o f_s^2} \cdot \left( \frac{V_o}{\Delta V_o} \right) = 31.7 \mu\text{F} \quad (7)$$

input voltage, $V_B$	18 ~ 36 $V_{dc}$
output voltage, $V_o$	11.4 $V_{dc}$
maximum output current, $I_o$	2 A
ripple of output voltage, $\Delta V_o$	10 mV <sub>pp</sub>
switching frequency, $f_s$	150 kHz

Table 1. Electrical Specifications of the Prototype.

The standard capacitance with 33  $\mu\text{F}$  is selected for  $C_o$ .

Step 5-Determine  $n_1$ : Select core material as TDK PC40 and core size as EE-19. Its saturation flux density  $B_{sat}$  is 4500 G at 60 °C, and effective cross area  $A_e$  is 0.23  $\text{cm}^2$ . To avoid core saturation, we set the maximum flux density  $B_{max}$  at half of  $B_{sat}$ . Therefore, the turn number of primary winding  $n_1$  can be calculated as

$$n_1 = \frac{V_B D T_s}{2 B_{max} A_e} = 7.7 \quad (8)$$

In the illustrative case,  $n_1$  is set as 8. The inductance of  $L_m$  can be measured as 80  $\mu\text{H}$ .

Step 6-Determine  $L_r$ : According to the operation principle of Mode 6, the current  $i_{Lr}$  at  $t = t_6$  can be obtained from following

$$|i_{Lr}(t_6)| = \frac{D V_B}{2 L_m f_s} = 0.5 \text{ A} \quad (9)$$

To achieve ZVS operation of the main switch  $S_1$ , the inductance of  $L_r$  should meet following equation

$$L_r > \frac{C_{ds} V_B^2}{|i_{Lr}(t_6)|^2} \quad (10)$$

Considering that the intrinsic capacitor  $C_{ds}$  of IRF530 is 190 nF, the required inductance of  $L_r$  can be obtained as 438 nH.

Step 7-Determine  $C_c$ : To optimize the voltage stresses of  $C_c$ ,  $S_1$  and  $S_2$ , the period of the resonance occurring during  $S_1$  turning-off should

be longer than ten times of the turn-off time of  $S_1$ , which is expressed as

$$2\pi\sqrt{(L_r + L_m)C_c} \geq 10 \times (1-D) / f_s \quad (11)$$

Thus, the minimum capacitance of  $C_c$  can be obtained as

$$C_c \geq \frac{100(1-D)^2}{(L_r + L_m)(2\pi f)^2} = 350\text{nF} \quad (12)$$

The standard capacitance with 470 nF is selected for  $C_c$ .

The calculated component parameters of the illustrative example are summarized in table 2.

#### 4. Experimental results

While input voltage  $V_B$  is 24 V, figure 7 shows the measured waveforms of the output voltage  $V_o$  and the output inductor current  $i_{L_o}$  at full load operation. It can be seen that  $V_o$  is regulated at 11.41 V, and the average output current is 2.04 A, which are very close to the required specifications. The measured waveform of clamping capacitor voltage  $V_c$  according the driving signal  $V_{GS1}$  is shown in figure 8. It is obvious that resonance with the frequency determined by  $C_c$  and  $(L_r + L_m)$  occurs after the main switch  $S_1$  is turning off. In this time interval, the resonant current  $i_{L_r}$  transfers energy from  $L_m$  to  $C_c$ , and then restores energy to the input voltage source.

main switch, $S_1$	IRF530 (100V/10A)
auxiliary switch, $S_2$	IRF9540 (100V/19A)
diodes, $D_3, D_4$	SB1060 (60V/10A)
leakage inductor, $L_r$	438 nH
magnetizing inductor, $L_m$	80 $\mu$ H
clamping capacitor, $C_c$	0.47 $\mu$ F
output inductor, $L_o$	100 $\mu$ H
output capacitor, $C_o$	33 $\mu$ F
transformer turn ratio, n:1	1:1

Table 2. Component Parameters of the Prototype.

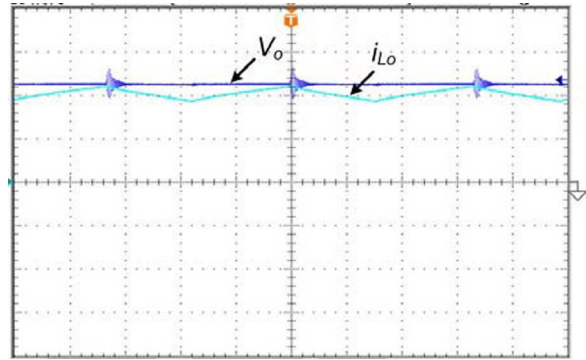


Figure 7. Measured waveforms of the output voltage  $V_o$  and the output inductor current  $i_{L_o}$  at full load operation ( $V_o$ : 5 V/div;  $i_{L_o}$ : 1 A/div; time: 2  $\mu$ s/div).

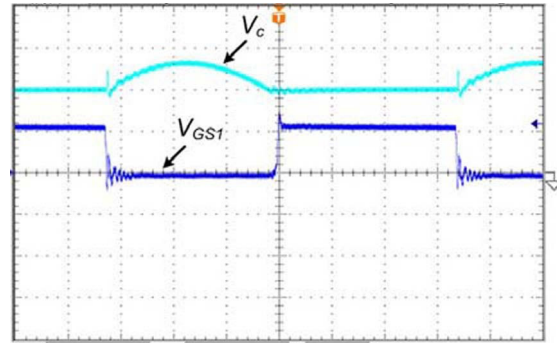


Figure 8. Measured waveforms of clamping capacitor voltage  $V_c$  according the driving signal  $V_{GS1}$  ( $V_{GS1}$ : 10 V/div;  $V_c$ : 20 V/div; time: 1  $\mu$ s/div).

Figure 9 shows the measured voltage and current waveforms of the main switches  $S_1$  at full load condition. It could be observed that  $S_1$  can turn on under ZVS condition. Figure 10 shows the measured voltage waveforms of the auxiliary switches  $S_2$  at full load condition. The drain to source voltage  $v_{ds2}$  becomes zero before the driving signal  $V_{GS2}$  is supplied, from which the ZVS operation of  $S_2$  can be verified. Therefore, the switching losses can be significantly minimized to improve system efficiency.

Figure 11 shows the measured efficiency curve of the proposed color LED driver with 24 V input voltage. The maximum efficiency is up to 92.5% at  $I_o = 1.6$  A. The normal operating range for driving color LED arrays is from 1.2 A to 1.8 A. The system efficiency can be kept above 91% in this range, which provide energy saving significantly.

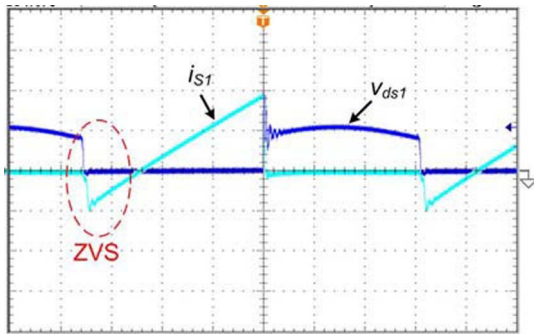


Figure 9. Measured voltage and current waveforms of the main switch  $S_1$  at full load operation ( $V_{ds1}$ : 50 V/div;  $i_{S1}$ : 5 A/div; time: 1  $\mu$ s/div).

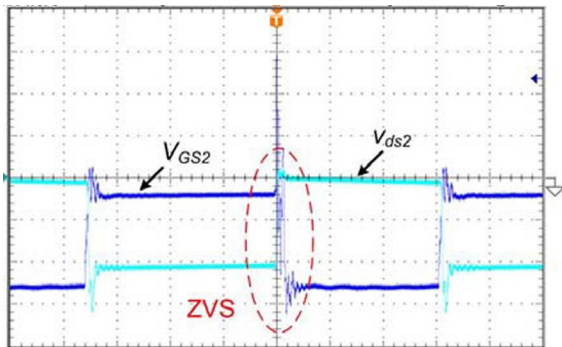


Figure 10. Measured voltage waveforms of the auxiliary switch  $S_2$  at full load operation ( $V_{ds2}$ : 20 V/div;  $V_{GS2}$ : 5 V/div; time: 1  $\mu$ s/div).

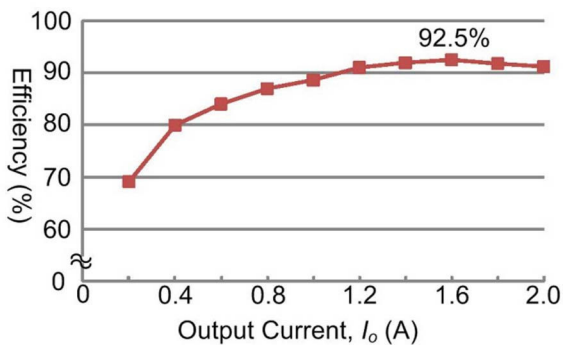


Figure 11. Measured efficiency curve of the proposed color LED driver.

Figure 12 shows the measured waveforms of output voltage  $V_o$  and output current  $I_o$  while the LED module outputs “white” light. It can be seen

that red, green, and blue LED arrays are driving in sequential and with the frequency of 30 Hz. The output voltage  $V_o$  is around 10.4 V for driving red LEDs, and  $V_o$  is regulated to around 11.4 V for driving green and blue LEDs. The duty cycle of each LED is almost 100% so that all of them provide the highest luminance to have “white” light output. In figure 13, the duty cycle of green LEDs is changed to be 50% to reduce the luminance. Since the luminance of red and blue LEDs remain 100%, the color of the light provided by LED modules is “purple”. These experimental results verified that a large chromaticity variation can be achieved by low-frequency PWM control. By the way, the photo of the illustrative prototype is shown in figure 14.

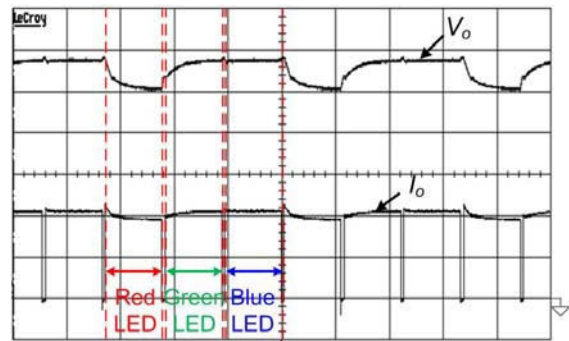


Figure 12. Measured waveforms of output voltage  $V_o$  and output current  $I_o$  while the LED module outputs “white” light ( $V_o$ : 2 V/div;  $I_o$ : 500 mA/div; time: 10 ms/div).

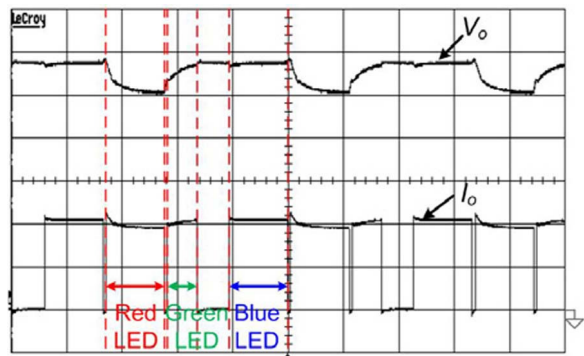


Figure 13. Measured waveforms of output voltage  $V_o$  and output current  $I_o$  while the LED module outputs “purple” light ( $V_o$ : 2 V/div;  $I_o$ : 500 mA/div; time: 10 ms/div).



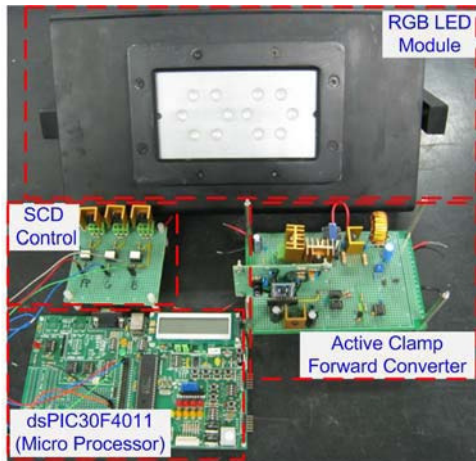


Figure 14. Illustrative prototype of the proposed color LED driver.

## 5. Conclusion

An active clamp forward converter with the SCD control for driving RGB LED arrays has been proposed. ZVS turn-on operations of both the main switch and the auxiliary switch lead to low switching losses and high system conversion efficiency. RGB LED arrays are sequentially driven by the same converter, which can save components and reduce cost significantly. Besides, PWM control is applied to achieve a large chromaticity variation. Experimental results of a 100 W illustrative example have really proved the feasibility and validity of the theoretical predictions.

## Acknowledgements

This work was supported by the National Science Council of Taiwan, Republic of China, under grant contract NSC 101-2221-E-214-059.

## References

- [1] G. Harbers et al., "Performance of high power light emitting diodes in display illumination applications," *J. Disp. Technol.*, vol. 3, no. 2, pp. 98–109, Jun. 2007.
- [2] S. Muthu et al., "Red, green, and blue LEDs for white light illumination," *IEEE J. Sel. Top Quant.*, vol. 8, no. 2, pp. 333–338, Mar. / Apr. 2002.
- [3] W.-C. Cheng, "Power minimization of LED backlight in a color sequential display," *J. Soc. Inf. Display*, vol. 36, no. 1, pp. 1384–1387, May 2005.

- [4] F. Gatti et al., "Low power control technique for TFT LCD display," in *proceedings of Compilers, Architecture, and Synthesis for Embedded System*, 2002, pp. 218–224.

- [5] C.-C. Chen et al., "Sequential color LED backlight driving system for LCD panels," *IEEE T. Power Electr.*, vol. 22, no. 3, pp. 919–925, May 2007.

- [6] Y.-K. Lo et al., "Design and implementation of RGB LED drivers for LCD backlight modules," *IEEE T. Ind. Electron.*, vol. 56, no. 12, pp. 4862–4871, Dec. 2009.

- [7] C. M. C. Duarte and I. Barbi, "A family of ZVS-PWM active-clamping DC-to-DC converters: synthesis, analysis, design, and experimentation," *IEEE T. CIRCUITS-I*, vol. 44, no. 8, pp. 698–704, Aug. 1997.

- [8] A. Acik and I. Cadirci, "Active clamped ZVS forward converter with soft-switched synchronous rectifier for high efficiency, low output voltage applications," *IET Electr. Power App.*, vol. 150, no. 2, pp. 165–174, Mar. 2003.

- [9] Q. M. Li and F. C. Lee, "Design consideration of the active-clamp forward converter with current mode control during large-signal transient," *IEEE T. Power Electr.*, vol. 18, no. 4, pp. 958–965, Jul. 2003.